Acta Crystallographica Section B
Structural Science
ISSN 0108-7681

Order and disorder among the layered double hydroxides: combined Rietveld and *DIFFaX* approach

A. V. Radha,[a] P. Vishnu Kamath[a]* and C. Shivakumara[b]

[a]Department of Chemistry, Central College, Bangalore University, Bangalore 560 001, India, and [b]Solid State and Structural Chemistry Unit, Indian Institute of Science, Bangalore 560 012, India

Correspondence e-mail: vishnukamath8@hotmail.com

Received 14 November 2006
Accepted 10 January 2007

A combined approach using the Rietveld technique of structure refinement and *DIFFaX* simulations of the powder patterns enables us to not only arrive at the complete structure of the layered double hydroxides (LDHs), but also classify and quantify the nature of structural disorder. Hydrolysis of urea dissolved in mixed-metal salt solutions containing a divalent metal (Mg^{2+}, Co^{2+}) with Al^{3+} results in the homogeneous precipitation of the corresponding LDH. The products obtained are highly crystalline enabling a complete structure determination including subsequent refinement by the Rietveld method. In contrast, the LDH of Ni^{2+} with Al^{3+} crystallizes with the incorporation of stacking faults. A combined Rietveld–*DIFFaX* approach shows that even 'crystalline' samples of this LDH incorporate up to 9% of stacking faults, which are not eliminated even at elevated temperatures (473 K). These studies have implications for the order, disorder and 'crystallinity' of layered phases in general and metal hydroxides in particular.

1. Introduction

Laboratory synthesized layered double hydroxides (LDHs) obtained by coprecipitation at different pH values are replete with stacking faults (Bellotto *et al.*, 1996; Drits & Bookin, 2001; Thomas *et al.*, 2004; Radha *et al.*, 2005). Stacking faults are incorporated during the precipitation process itself and once incorporated cannot be eliminated by hydrothermal treatment (Bellotto *et al.*, 1996; Radha *et al.*, 2005). Stacking faults in layered materials are very special in that the atoms involved in these planar defects have the same coordination symmetry as well as coordination number as those in the ordered domains of the crystal (Verma & Krishna, 1966). Consequently, stacking faults contribute to the thermodynamic stability by enhancing the entropy of the crystal, while not depleting the enthalpy of the system. Further, specific kinds of stacking faults facilitate the inclusion of carbonate ions by retaining the local symmetry of the interlayer sites and thereby preserving the hydrogen-bonding interactions between the intercalated species and the metal hydroxide slabs (Taylor, 1973; Bookin & Drits, 1993). On account of the thermodynamic stability mediated by the intercalated carbonate anions, the stacking faults persist even on hydrothermal treatment and in some instances such as the carbonate-containing LDH of Co with Fe ($Co-Fe-CO_3^{2-}$), decomposition precedes any structural ordering. The presence of structural disorder manifests itself in the non-uniform broadening of select families of reflections in the X-ray powder diffraction patterns of the samples. In particular, stacking faults selectively broaden the peaks due to the $0k\ell$ family of reflections (Bellotto *et al.*, 1996; Drits & Bookin, 2001; Thomas *et al.*, 2004; Radha *et al.*, 2005). Struc-

ture refinement by the Rietveld method using X-ray powder diffraction data is therefore fraught with much uncertainty.

It is therefore a considerable challenge to synthesize the ordered LDHs of Mg, Co and Ni with Al. Many authors report the synthesis of LDHs and proceed to apply the Rietveld technique of structure refinement (Bellotto *et al.*, 1996; Ennadi *et al.*, 1994, 2000). Although the Rietveld fits are satisfactory, it is our opinion that these are purely the results of a mathematical fit of experimental data rather than being indicative of the actual structure. As long as various families of Bragg reflections are non-uniformly broadened, there are serious limitations to the structural interpretations that these fits afford.

Confronted with these difficulties, many authors have resorted to novel methods of choosing the profile function and introducing additional parameters to alter the shape of the profile function. These additional parameters are then interpreted in terms of structural disorder. Thus, Deabate *et al.* (2000) introduce additional parameters in their profile function to fit the experimentally observed broadening of Bragg peaks in the X-ray powder diffraction patterns of nickel hydroxide. They attribute the additional broadening to a specific kind of disorder, which in our opinion corresponds to interstratification. Interstratification is the loss of periodicity in the stacking direction. In nickel hydroxide this arises due to the random insertion of water molecules in the interlayer region. However, among the LDHs, the major contribution to structural disorder comes from stacking faults. The effect of stacking faults on the X-ray powder diffraction pattern of the LDH of Ni with Al was first simulated by Hines *et al.* (1997) using the *DIFFaX* technique (Treacy *et al.*, 1991, 2000). They attributed the non-uniform broadening of peaks to the random orientation of successive layers about the crystallographic *c* axis, a type of disorder known as 'turbostraticity'.

For the purpose of structure refinement by the Rietveld method, highly ordered samples are required. The peaks corresponding to the Bragg reflections in the X-ray powder diffraction patterns of such samples are not only expected to be narrow, but also exhibit uniform line broadening.

2. Experimental

Solid urea was added to 40 ml of a 0.5 *M* mixed-metal ($M^{II} + Al^{III}$) nitrate solution maintaining the urea/($M^{II} + Al^{III}$) molar ratio at 3.3. The clear solutions obtained were heated at different temperatures between 353 and 473 K for 24 h. Heating above the boiling point of water was carried out in a teflon-lined autoclave under autogenous pressure. The solids were recovered by filtration, copiously washed to constant pH and then dried at 353 K.

All the samples were characterized by X-ray powder diffraction using an X'pert Pro Philips diffractometer (source Cu $K\alpha$, λ = 1.541 Å) operated in a reflection geometry and fitted with a graphite secondary monochromator. Data were collected using a continuous scan rate of 2° 2θ min^{-1}, which were then rebinned into 2θ steps of 0.02° 2θ. The instrumental broadening of the Bragg peaks is estimated to be 0.15–0.2° of 2θ in the 77–28° range of 2θ for the Si standard. Any broadening of the peaks beyond this value was attributed to the sample. To confirm the presence of intercalated carbonate anions, IR spectroscopic studies were carried out on all the samples using a Nicolet model Impact 400D FTIR spectrometer (4000–400 cm^{-1}; resolution 4 cm^{-1}, KBr pellet).

3. Computational studies

3.1. Rietveld refinement

The Rietveld refinement technique was used for structure refinement (*FULLPROF*; Rodriguez-Carvajal, 2005). In all the refinements, the modified pseudo-Voigt line-shape function with five variables (*U*, *V*, *W*, *X* and η) was used to fit the experimental profiles. Refinements were also carried out with profiles incorporating the Pearson VII correction for comparing the effect of profile function on the quality of the fit and the difference profile. The background adjustment in the calculated patterns was made using a 12 polynomial function. The crystal structure of mineral hydrotalcite was chosen as the model (ICSD No. 6296, space group: $R\bar{3}m$, a = 3.054, c = 22.81 Å) for the Rietveld refinement of the structures of the $M-Al-CO_3^{2-}$ LDHs (M = Ni^{2+}, Co^{2+}). For M = Mg^{2+}, a more recent model structure (CC-81963, space group: $R\bar{3}m$, a = 3.046, c = 22.772 Å) was used (Bellotto *et al.*, 1996).

3.2. *DIFFaX* simulations

In instances where the X-ray powder diffraction pattern exhibited non-uniform broadening of select families of reflections owing to structural disorder, *DIFFaX* (Version 1.807; Treacy *et al.*, 1991, 2000) simulations of the PXRD (powder X-ray diffraction) patterns were employed for the quantification of disorder. The details of the *DIFFaX* simulations of LDHs are given elsewhere (Thomas *et al.*, 2004; Radha *et al.*, 2005). For the purpose of *DIFFaX* simulations, the layer was described according to the model structure. Each layer comprises a metal hydroxide slab and the atoms of the interlayer and can be represented as *AbCX*. Here *A* and *C* represent the hydroxyl ion positions and *b* represents the cations in octahedral sites. *X* represents the position of the interlayer atoms. When these layers are stacked one above another using the stacking vector (0, 0, 1) an ordered single-layer thick hexagonal structure is obtained having the hydroxyl ion stacking sequence *AC AC AC*–. Successive translations of the *A* site by the vector (2/3, 1/3) carries $A \Rightarrow C$, $B \Rightarrow A$ and $C \Rightarrow B$. Applying the translations to the *AC* layer yields the stacking sequence *AC CB BA AC*–, a triple layered lattice having rhombohedral symmetry and given the symbol $3R_1$ (Bookin & Drits, 1993). When two layers of the type *AC* and *CA* are stacked one above another to yield the stacking pattern *AC CA AC*–, a two-layer polytype is obtained and is given the symbol $2H_1$ (Bookin & Drits, 1993). A random mix of these stacking patterns may be obtained starting with one (*AC*) or more (*AC* and *CA*) layers and by the simultaneous use of more than one stacking vector with predetermined probabilities. This results in a lattice with stacking faults, but

nevertheless comprising trigonal prismatic interlayer sites exclusively. These sites facilitate the inclusion of carbonate ions in the interlayer. The calculated reflections are broadened using a Lorentzian profile function to facilitate comparison with the observed pattern. The FWHM of the Lorentzian was obtained from the width of the 110 reflection which remains unaffected by structural disorder (Thomas *et al.*, 2004). The stacking fault probabilities were varied by hand until the peaks in the simulated pattern were matched with those in the observed pattern to within $\pm 0.1^\circ$ 2θ for position and FWHM, and within $\pm 5\%$ in relative intensity.

Where *DIFFaX* simulations are used in tandem with Rietveld refinement, the pseudo-Voigt line-shape parameters refined by the Rietveld technique are input into the *DIFFaX* simulations. In these instances, the R_{wp} value was evaluated to find the goodness-of-fit of the *DIFFaX* simulation. Illustrative input files used in the *DIFFaX* simulations of the X-ray powder diffraction patterns of the $3R_1$ and $2H_1$ polytypes, as well as the simulation of the pattern of the faulted crystal are included as supplementary information.[1]

4. Results and discussion

LDHs are derived from the structure of the mineral brucite, $Mg(OH)_2$ (Cavani *et al.*, 1991). Brucite itself comprises a hexagonal packing of hydroxyl ions with Mg^{2+} ions occupying alternate layers of octahedral sites. This pattern of cation distribution results in a stacking of charge-neutral metal hydroxide slabs of the composition $[Mg(OH)_2]$ (Oswald & Asper, 1977). When a fraction, x, of the Mg^{2+} ions are isomorphously substituted by a trivalent ion such as Al^{3+}, the layers acquire a composition $[Mg_{1-x}Al_x(OH)_2]^{x+}$. A positive charge develops on the metal hydroxide slab, to neutralize which anions, most commonly CO_3^{2-}, are incorporated in the interlayer region along with water molecules (Khan & O'Hare, 2002). All metal hydroxides except those of alkali metals and the heavier alkaline earth metals are insoluble with solubility products ranging from 10^{-10} to 10^{-36} (Dobos, 1975). Unitary metal hydroxides such as those of Mg, Ni and Co are therefore prepared by strong alkali precipitation from the solution of a suitable metal salt (Hui *et al.*, 1995). By an extension of this practice the LDHs are also prepared by strong alkali or ammonia precipitation from a mixed-metal salt solution (Reichle, 1986; Boclair & Braterman, 1998, 1999; Olanrewaju *et al.*, 2000).

Many factors control the outcome of a precipitation reaction, with a rather profound affect on crystallinity and phase formation. Grosso *et al.* (1992) have comprehensively studied the affect of all these parameters on the synthesis of the Cu–Cr LDH. Chief among the parameters varied are the pH at precipitation and the temperature.

(i) The non-uniform broadening of peaks in the PXRD patterns of layered hydroxides is not entirely due to particle anisotropy (Ramesh *et al.*, 2003; Thomas & Kamath, 2006). An uncritical use of the Scherrer formula leads to unrealistic estimates of particle size.

(ii) Our earlier work (Radha *et al.*, 2005) has shown that the LDHs incorporate stacking faults during the precipitation reaction and the extent of stacking faults varies with the pH at precipitation. For instance, the Co–Al–CO_3^{2-} LDH precipitated at low pH values (~ 8) incorporates a smaller percentage (20%) of stacking faults compared with the LDH precipitated under other conditions (pH = 10; 55%). However, the pH at precipitation cannot be reduced below the critical value, which corresponds to the LDH-formation pH.

(iii) At low pH values, carbonates undergo decomposition and a mix of different anions is incorporated in the interlayer region. This itself becomes a source of disorder, as different anions have different van der Waals radii and tend to destroy the periodicity along the crystallographic c axis – a kind of disorder known as 'interstratification' (Demourgues & Delmas, 1996).

(iv) The incorporation of anions, whose symmetry does not match with the symmetry of the interlayer site in the LDH introduces turbostratic disorder (Hines *et al.*, 1997). The trigonal prismatic interlayer sites in the LDHs are symmetry matched with the carbonate ions of the D_{3h} symmetry. While CO_3^{2-} ions have the potential to introduce structural order, anions of other symmetry as well as those of lower charge produce structural disorder.

(v) Stacking disorders, including turbostraticity, once incorporated cannot be eliminated by methods such as hydrothermal treatment.

As an illustration of this last factor, Fig. 1 shows the X-ray powder diffraction patterns of the Ni–Al–CO_3^{2-} LDH obtained before (pH > 12; 353 K) and after hydrothermal treatment (453 K, 24 h, 50% filling). Fig. 2 shows the *DIFFaX*

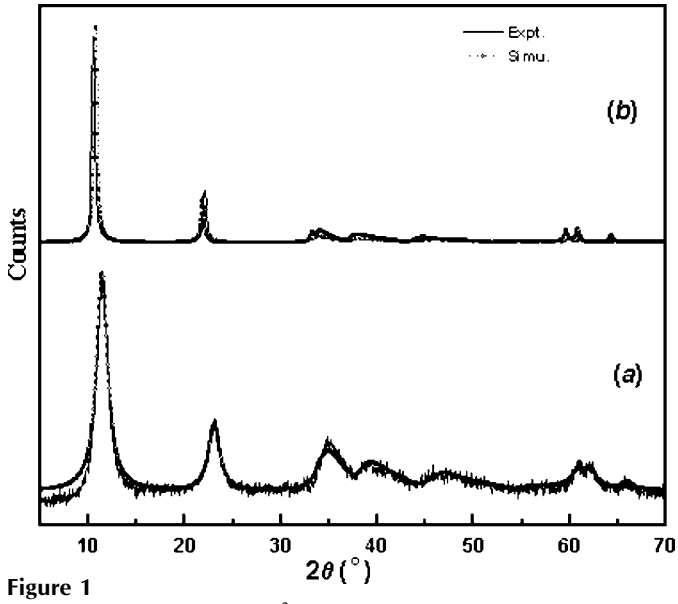

Figure 1
PXRD patterns of Ni–Al–CO_3^{2-} LDH precipitated at pH > 12 (*a*) before and (*b*) after hydrothermal treatment compared with the corresponding *DIFFaX* simulations.

[1] Supplementary data for this paper are available from the IUCr electronic archives (Reference: LM5004). Services for accessing these data are described at the back of the journal.

Table 1
Results of *DIFFaX* simulations of the PXRD patterns of the Ni–Al–CO_3^{2-} LDHs.

Ni–Al–CO_3^{2-} LDH	$3R_1$ (%)	$2H_1$ (%)	Lorentzian (°2θ)	No. of layers
Coprecipitated (353 K)	50	50	1.4	∞
Coprecipitated, HT 453 K	50	50	0.4	∞
HPFS, 373 K	75	25	0.6	∞
HPFS, HT 413 K	90	10	0.6	20
HPFS, HT 453 K	93	7	0.3	40
HPFS, HT 473 K	91	9	–†	∞

† Pseudo-Voigt profile obtained from the Rietveld refinement shown in Fig. 7 is used here.

simulated X-ray powder diffraction patterns expected of model structures belonging to the $2H_1$ and $3R_1$ polytypes. Although the peak positions in the observed pattern match with those in the pattern expected of the $3R_1$ polytype, the excessive and selective broadening of the $0k\ell$ reflections is evident. The observed patterns were simulated by incorporating 50% of $2H_1$ stacking motifs within the matrix of the $3R_1$ polytype. The *DIFFaX* simulated patterns are also shown in Fig. 1. The only difference observed subsequent to hydrothermal treatment is a narrowing of the basal reflections. Therefore, the FWHM of the Lorentzian profile function used in the simulation of the hydrothermally treated sample (0.4° 2θ) is lower than that used for the as-prepared sample (1.4° 2θ). A smaller Lorentzian line width is indicative of crystal growth, which is expected on hydrothermal processing. The percentage incidence of stacking faults remains unchanged at 50% (see Table 1 for the results of the *DIFFaX* simulations).

The formation of a solid from a solution takes place by nucleation and growth. Zhao *et al.* (2002) modified the synthesis of the Mg–Al LDH in such a way as to separate the nucleation step from the growth step by high-speed stirring of the slurry during precipitation. However, this did not make any difference to the crystallinity of the product as shown by the selective broadening of the $0k\ell$ reflections in the X-ray powder diffraction patterns recorded by them. Such broadening arising from the random intergrowth of the $3R_1$ and $2H_1$ polytypes (as shown in Fig. 1) is commonly observed and reported by numerous authors (Martin *et al.*, 1999; Tichit *et al.*, 2002; Seida *et al.*, 2002).

Another factor affecting product formation is the precipitation kinetics. A convenient method of altering the kinetics of precipitation is by the controlled release of alkali by hydrolysis of urea (Costantino *et al.*, 1998, 1999; Ogawa & Kaiho, 2002; Adachi-Pagano *et al.*, 2003). Urea hydrolysis results in

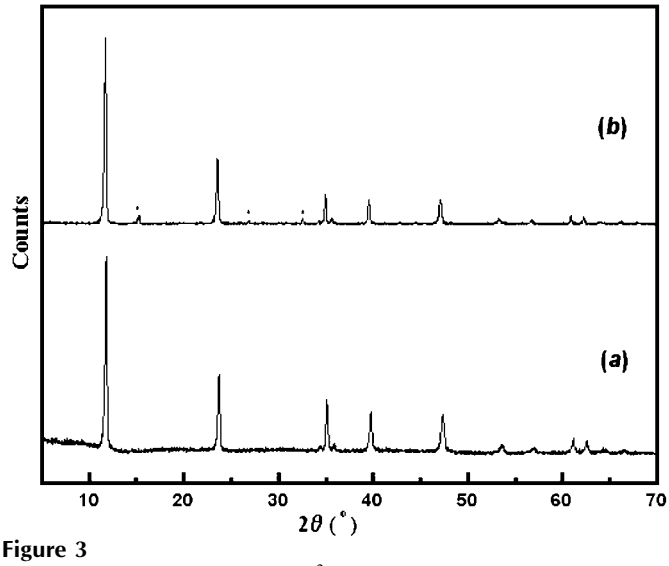

Figure 3
PXRD patterns of the Mg–Al–CO_3^{2-} LDH obtained by urea hydrolysis at (*a*) 353 K and (*b*) 413 K, respectively. Peaks marked by an asterisk are due to impurities.

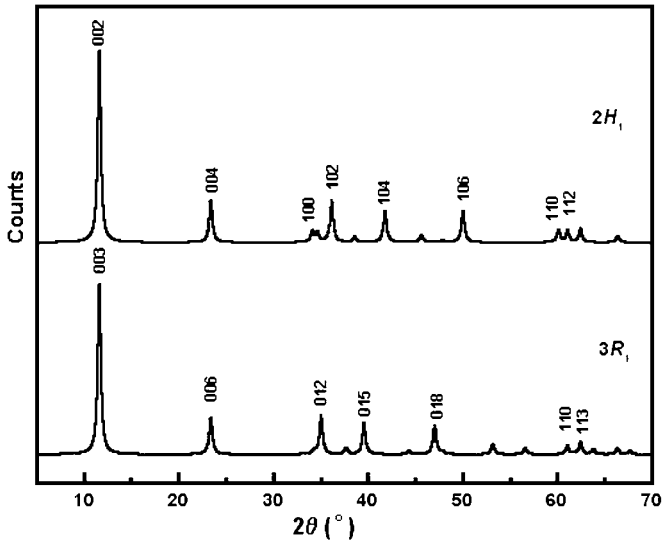

Figure 2
DIFFaX simulations of model structures belonging to the $3R_1$ and $2H_1$ polytypes.

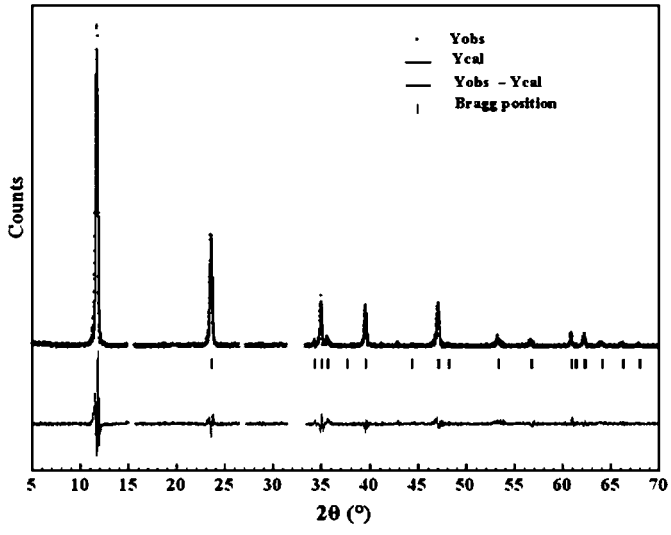

Figure 4
Results of the Rietveld refinement of the structure of the Mg–Al–CO_3^{2-} LDH using the X-ray powder diffraction pattern given in Fig. 3(*b*). The impurity peaks have been excluded in the profile-fitting procedure.

Table 2
Results of the Rietveld refinements of the Mg–Al, Co–Al and Ni–Al LDHs.

	$Mg_4Al_2(OH)_{12}CO_3{\cdot}3H_2O$	$Co_4Al_2(OH)_{12}CO_3{\cdot}3H_2O$	$Ni_6Al_2(OH)_{16}CO_3{\cdot}\ 4H_2O$
Space group	$R\bar{3}m$	$R\bar{3}m$	$R\bar{3}m$
Cell parameters			
a (Å)	3.0424 (2)	3.0660 (2)	3.0336 (2)
c (Å)	22.664 (4)	22.593 (2)	22.848 (2)
Shape parameters			
U	0.042 (6)	0.13 (8)	0.779251
V	−0.07 (4)	−0.01 (4)	−0.265 (6)
W	0.069 (5)	0.051 (4)	0.131 (1)
X	0.005 (2)	0.008 (2)	0.000000
η	0.31 (4)	0.32 (4)	0.931 (9)
Goodness-of-fit			
R_{wp}	0.403	0.371	0.235
R_{Bragg}	0.1029	0.0894	0.0547
R_F	0.1344	0.0945	0.0533
R_p	0.326	0.324	0.314
χ^2	0.0374	0.0153	0.0238
Distances (Å)			
(M,Al)—O1	1.991 (4)	2.003 (4)	–†
O1—O1	2.569 (9)	2.578 (9)	
O1—O2	2.915 (9)	2.895 (9)	
C—O2	1.098 (11)	1.154 (11)	
Angles (°)			
O1—(M,Al)—O1	80.4 (4)	80.1 (4)	–†
O1—(M,Al)—O1	99.64 (17)	99.89 (17)	
O2—C—O2	120.0 (9)	120.0 (8)	

† Data not given since it is a faulted sample.

the generation of NH_3 on one hand and CO_3^{2-} ions on the other. The former provides the alkaline pH, while the latter helps in the ordered stacking of the hydroxide layers. This method is known as homogeneous precipitation from solution (HPFS). The kinetics of precipitation can be varied by carrying out the hydrolysis at different temperatures (373–473 K) in an autoclave.

Fig. 3 shows the X-ray powder diffraction patterns of the Mg–Al–CO_3^{2-} LDH obtained at 353 and 413 K, respectively. In complete contrast to literature reports (Bellotto *et al.*, 1996; Drits & Bookin, 2001; Thomas *et al.*, 2004; Radha *et al.*, 2005; Martin *et al.*, 1999; Tichit *et al.*, 2002; Seida *et al.*, 2002) and those patterns shown in Fig. 1, the X-ray powder diffraction patterns of both products show sharp Bragg reflections. Most noteworthy are the FWHM values ($0.2 \pm 0.05^\circ$ 2θ) of the peaks appearing in the mid 2θ region, where the $0k\ell$ reflections arise. These values are comparable with the instrumental contribution measured for the Si standard showing that there is little, if any, sample-related broadening. The sample obtained at 413 K exhibits minor reflections corresponding to an unspecified impurity phase, formed either by the decomposition of the LDH or by the serial precipitation of $Al(OH)_3$ at a lower pH than the LDH precipitation pH (Radha & Kamath, 2003). Fig. 4 shows a Rietveld refinement of the structure of the Mg–Al–CO_3^{2-} using the X-ray powder diffraction data shown in Fig. 3(*b*), excluding the regions where the impurity-related peaks arise. The refinement is satisfactory and the results are given in Tables 2 and 3.

Fig. 5 shows the X-ray powder diffraction pattern of the Co–Al–CO_3^{2-} (413 K) LDH along with the results of the Rietveld refinement. Here too the fit is satisfactory (see Tables 2 and 3).

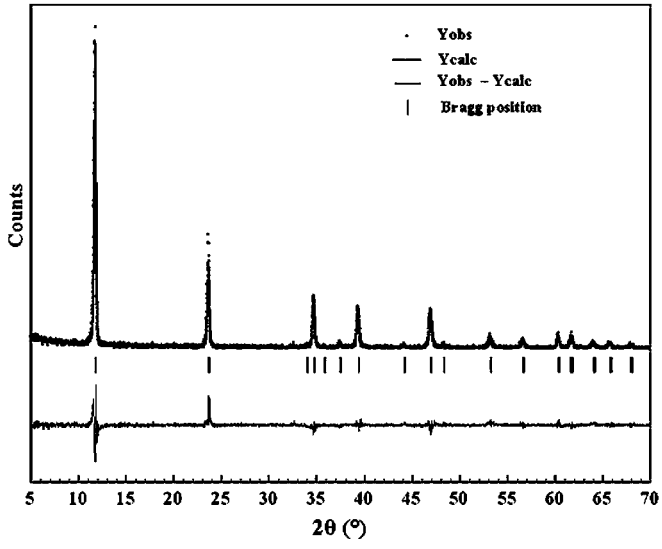

Figure 5
Results of the Rietveld refinement of the structure of the Co–Al–CO_3^{2-} LDH.

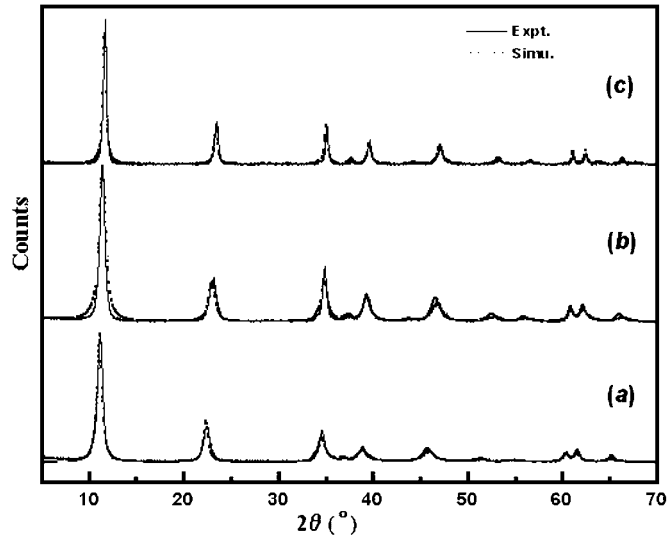

Figure 6
PXRD patterns of the Ni–Al–CO_3^{2-} LDH obtained by urea hydrolysis at (*a*) 373, (*b*) 413 and (*c*) 453 K. The corresponding *DIFFaX* simulations are also shown.

Table 3
Position parameters obtained from the Rietveld refinements of the Mg–Al and Co–Al LDHs.

	Atom	Site	x	y	z	B_{iso}(Å^2)
$Mg_4Al_2(OH)_{12}CO_3{\cdot}3H_2O$	Mg	3(*a*)	0.000	0.000	0.0000	0.000
	Al	3(*a*)	0.000	0.000	0.0000	0.000
	O1	6(*c*)	0.000	0.000	0.3747 (4)	0.000
	C	6(*c*)	0.3333	0.6667	0.5000	0.000
	O2	18(*h*)	0.125 (3)	−0.125 (3)	0.5000	0.000
$Co_4Al_2(OH)_{12}CO_3{\cdot}3H_2O$	Co	3(*a*)	0.000	0.000	0.0000	1.1 (4)
	Al	3(*a*)	0.000	0.000	0.0000	1.1 (4)
	O1	6(*c*)	0.000	0.000	0.3747 (4)	0.0000
	C	6(*c*)	0.0000	0.0000	0.167	0.0000
	O2	18(*h*)	0.116 (3)	−0.116 (3)	0.5000	0.0000

Table 4
FWHM values of reflections observed in the PXRD patterns of the Ni–Al–CO_3^{2-} LDHs obtained by urea hydrolysis at different temperatures.

	FWHM† in ° 2θ			
hkℓ	373 K	413 K	453 K	473 K
003	0.7	0.6	0.4	0.4
006	0.7	0.8	0.5	0.4
012	0.6	0.6	0.4	0.3
015	0.9	0.9	0.5	0.4
018	1.1	1.2	0.5	0.6
110	0.7	0.6	0.4	0.4
113	0.8	0.7	0.4	0.4

† Measured to within 0.1° 2θ.

In this system synthesis at 453 K led to the formation of other phases unrelated to the LDH.

The Ni–Al LDH was interesting as in this case, the gradual elimination of stacking disorders could be detected in a cohort of samples prepared by the urea hydrolysis method in the 373–453 K range. Fig. 6 shows a representative set of X-ray powder diffraction patterns of the Ni–Al–CO_3^{2-} LDH obtained at various temperatures. It is evident that even at 373 K, the product of urea hydrolysis yields a pattern with sharp peaks compared with those in Fig. 1. This feature is in general reflective of a more ordered set of samples. However, the peaks due to the various reflections are non-uniformly broadened (see Table 4). Furthermore, the FWHM values of the peaks progressively decrease in samples obtained at higher temperatures. This kind of non-uniform broadening is indicative of structural disorder and therefore the patterns were subjected to analysis by *DIFFaX*. The corresponding *DIFFaX* simulations are also shown in Fig. 6. The results of the simulations are summarized in Table 1. *DIFFaX* simulations show that the incidence of stacking faults progressively decreases from 25% at 373 K to 7% in the sample obtained at 453 K. A comparison of these results with those in Fig. 1 shows that the progressive reduction in the incidence of stacking disorders with increasing temperature of precipitation is on account of the enhancement of the temperature at which nucleation takes place rather than due to growth and/or any disorder to order transformation.

It is evident that the stacking disorders are not completely eliminated even at 453 K. Therefore, another sample was prepared at 473 K. The PXRD pattern of this sample (see Fig. 7) was subjected to the Rietveld refinement procedure. Although the refinement is satisfactory (see Table 2), an examination of the difference profile shows that there is a systematic residual intensity under the 018 reflection. The refinement carried out by other authors (Bellotto *et al.*, 1996; Costantino *et al.*, 1998) also shows a systematic residual intensity in this region (30–50° 2θ) of the PXRD pattern. To verify if this feature in the

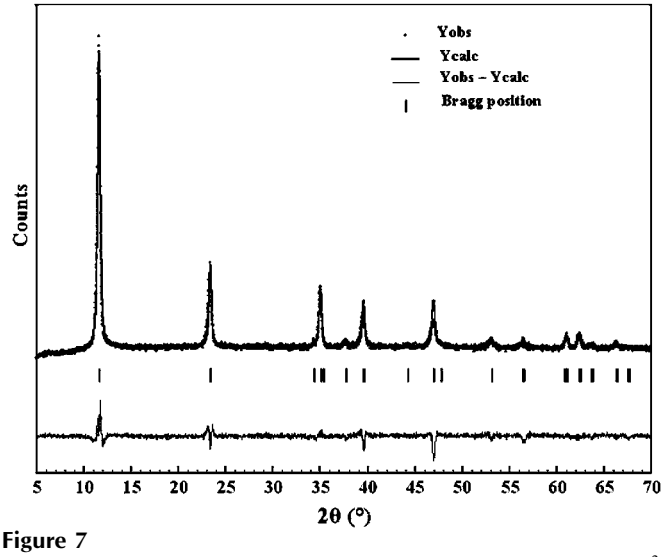

Figure 7
Results of the Rietveld refinement of the structure of the Ni–Al–CO_3^{2-} LDH obtained by urea hydrolysis at 473 K showing the systematic residual intensity in the difference profile.

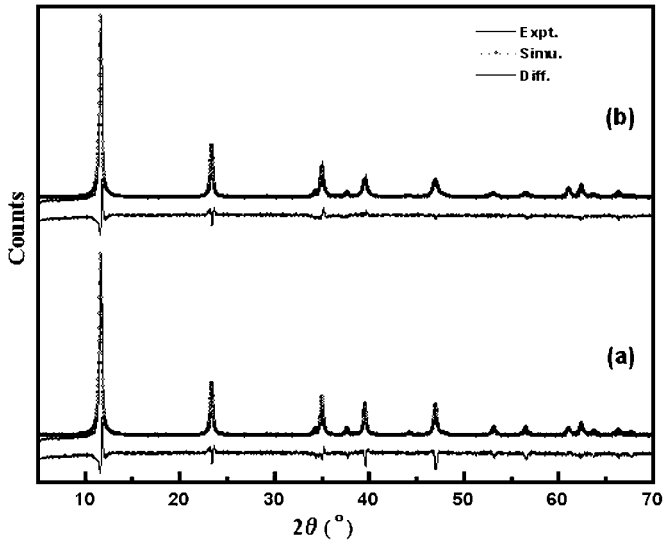

Figure 8
(*a*) *DIFFaX* simulation corresponding to the Rietveld refined structure of Fig. 7. (*b*) represents that shown in (*a*) with the inclusion of 9% stacking faults corresponding to the $2H_1$ polytypic motifs.

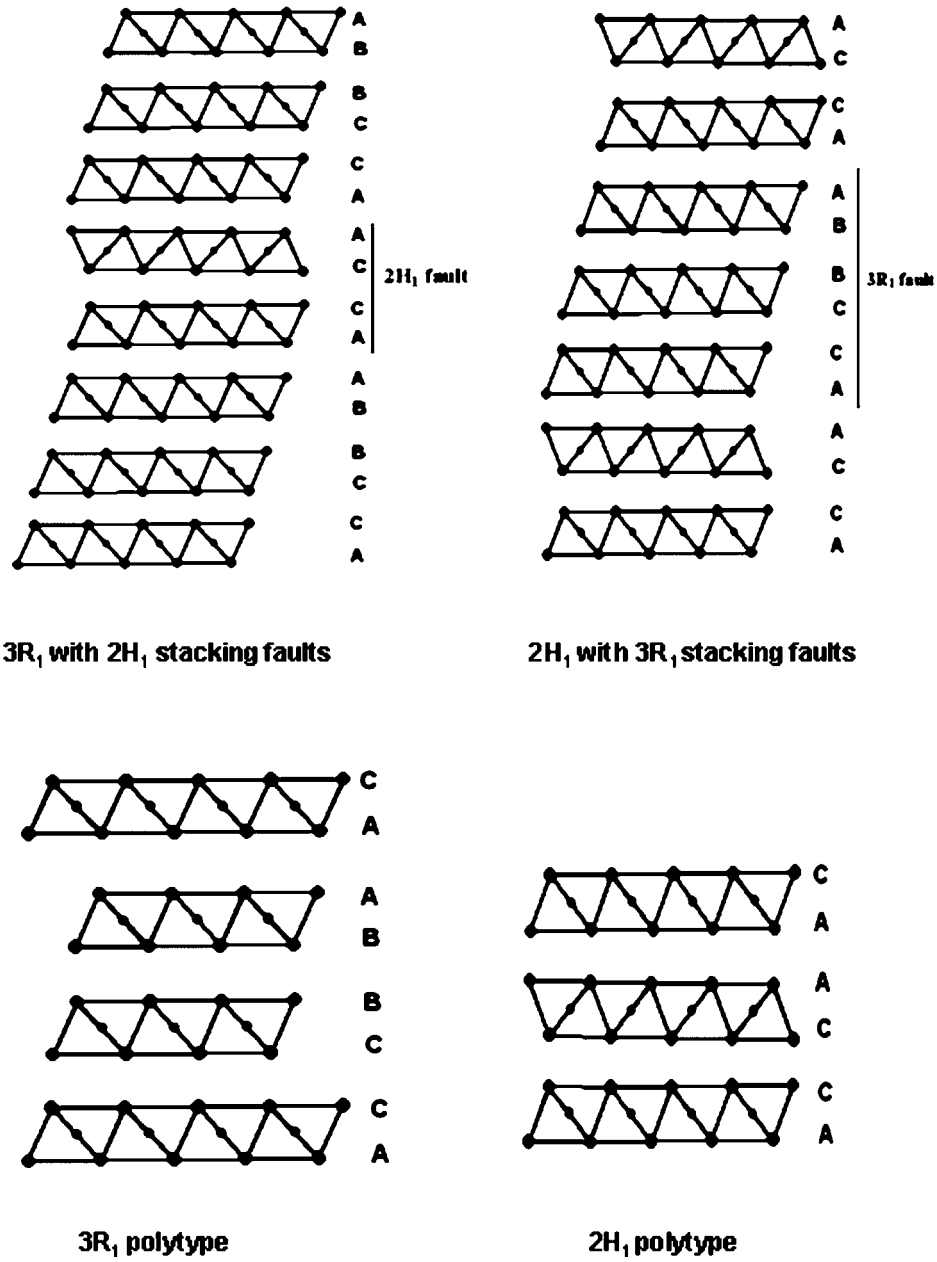

Figure 9
Schematic representations of different polytypes and the local structure of the faulted regions (interlayer atoms are removed for the purpose of clarity).

difference profile is an artifact of the refinement procedure, the refinement was also carried out with a wide choice of profile parameters such as by the inclusion of a shape parameter and the Pearson VII correction (Louër & Langford, 1988). This feature in the difference profile persists with all the profile functions (data not shown). Also, the difference profile could not be improved by refinement of atomic positions, occupancy factors and thermal parameters. As this region of the PXRD pattern is sensitive to the incidence of stacking disorders (Thomas *et al.*, 2004; Radha *et al.*, 2005), we attribute this feature in the difference profile to the presence of a residual number of stacking disorders. To quantify this, the output parameters of the Rietveld refinement shown in Fig. 7 were input into the *DIFFaX* program and the results of the simulation are shown in Fig. 8(*a*). The difference profile calculated for this simulation is similar in character to that seen in Fig. 7 showing that the two *FORTRAN*-based packages are internally consistent. We incorporated 9% of stacking disorders into the simulation. The results are given in Fig. 8(*b*) and it is at once evident that the systematic residual intensity in the difference profile has been corrected. The R_{wp} value also improved from 0.358 to 0.249 on inclusion of the stacking disorders. From this combined Rietveld–*DIFFaX* approach, it was evident that even 'ordered' preparations of LDHs were susceptible to the inclusion of a certain number of residual stacking disorders.

Given the ubiquitous nature of stacking faults among the LDHs, it is useful to visualize the local structure about a stacking fault using a schematic representation. Fig. 9 shows the stacking sequences of the pure $3R_1$ and $2H_1$ polytypes. Also shown are two illustrative stacking sequences representing the faulted region:

(i) *AC CB BA* <u>*AC CA AC*</u> *CB BA AC*– and

(ii) *AC CA* <u>*AC CB BA*</u> *AC CA AC*–.

The faulted regions are underlined. Sequence (i) represents a faulted region having the local structure corresponding to the $2H_1$ polytype growing within the matrix of the $3R_1$ polytype and sequence (ii) represents a faulted region having the local structure of the $3R_1$ polytype growing within the matrix of the $2H_1$ polytype. Other equivalent sequences can be envisaged. For instance, the sequence *AC CB* <u>*BA AB BA*</u> *AC CB BA AC*– is equivalent to (i) and *AC CA AC* <u>*CA AB BC*</u> *CA AC*– is equivalent to (ii). It may be seen that all the faulted regions incorporate trigonal prismatic interlayer sites.

The use of urea hydrolysis for the precipitation of unitary hydroxides of Co and Ni was first reported from this laboratory (Dixit *et al.*, 1996). The resultant products were ordered

forms of the α-modifications of $Ni(OH)_2$ and $Co(OH)_2$. Subsequently other authors extended this method for the synthesis of LDHs (Costantino *et al.*, 1999; Ogawa & Kaiho, 2002). They not only reported the synthesis of monodispersed particles of the LDHs, but also control over the aspect ratio of discoidal hydroxide particles that show liquid crystalline properties (Liu *et al.*, 2005). Costantino *et al.* (1998) report the formation of crystalline LDHs, but their conclusions are based on an examination of the FWHM values of the basal reflections 003 and 006. However, as shown in Fig. 1, line broadening of the basal reflections merely indicates the extent of crystal growth along the stacking direction. Disorders manifest themselves by the broadening of the $0k\ell$ reflections. We conclusively demonstrate the formation of the ordered LDHs by a combination of the Rietveld and *DIFFaX* techniques.

5. Conclusions

Homogeneous precipitation from solution (HPFS) carried out at different temperatures yields highly ordered LDHs of Mg, Co and Ni with Al. Product formation by precipitation takes place by the nucleation and growth mechanism. While there is no control over the kinetics of either step during a precipitation reaction brought by the addition of a strong alkali, the HPFS technique offers a delicate kinetic control over both steps. The temperature of hydrolysis determines the rate of generation of base affecting the rate of nucleation. Growth is dependent on the concentrations of various species in solution. Another important factor is the hydrolysis constant of the reagent chosen for HPFS. These factors have not yet been explored and there is much scope for future work. Another challenge would be an effective way of separating the nucleation and growth steps and independently influencing the kinetics of each step. The combined use of the Rietveld method of structure refinement together with *DIFFaX* simulations of the powder diffraction patterns gives insights into the nature of structural disorder that neither method can give on its own.

Authors thank the Department of Science and Technology (DST), Government of India (GOI) for financial support. AVR thanks the University Grants Commission, GOI, for the award of a Senior Research Fellowship (NET).

References

Adachi-Pagano, M., Forano, C. & Besse, J. P. (2003). *J. Mater. Chem.* **13**, 1988–1993.
Bellotto, M., Rebours, B., Clause, O., Lynch, J., Bazin, D. & Elkaim, E. (1996). *J. Phys. Chem.* **100**, 8527–8534.
Boclair, J. W. & Braterman, P. S. (1998). *Chem. Mater.* **10**, 2050–2052.
Boclair, J. W. & Braterman, P. S. (1999). *Chem. Mater.* **11**, 298–302.
Bookin, A. S. & Drits, V. A. (1993). *Clays Clay Miner.* **41**, 551–557.
Cavani, F., Trifiro, F. & Vaccari, A. (1991). *Catal. Today*, **11**, 173–301.
Costantino, U., Marmottini, F., Nocchetti, M. & Vivani, R. (1998). *Eur. J. Inorg. Chem.* pp. 1439–1446.
Costantino, U., Coletti, N. & Nocchetti, M. (1999). *Langmuir*, **15**, 4454–4460.
Deabate, S., Fourgeot, F. & Henn, F. (2000). *J. Power Sources*, **87**, 125–136.
Demourgues, L. G. & Delmas, C. (1996). *J. Electrochem. Soc.* **143**, 561–566.
Dixit, M., Subanna, G. N. & Kamath, P. V. (1996). *J. Mater. Chem.* **6**, 1429–1432.
Dobos, D. (1975). *Electrochemical Data: A Handbook for Electrochemists in Industry and Universities*, pp. 221–224. Amsterdam: Elsevier.
Drits, V. A. & Bookin, A. S. (2001). *Layered Double Hydroxides: Present and Future*, edited by V. Rives, pp. 39–92. New York: Novo Scientist.
Ennadi, A., Khaldi, M., de Roy, A. & Besse, J. P. (1994). *Mol. Cryst. Liq. Cryst.* **244**, 373.
Ennadi, A., Legrouri, A., de Roy, A. & Besse, J. P. (2000). *J. Solid State Chem.* **152**, 568–572.
Grosso, R. P., Suib, S. L., Weber, R. S. & Schubert, P. F. (1992). *Chem. Mater.* **4**, 922–928.
Hines, D. R., Seidler, G. T., Treacy, M. M. J. & Solin, S. A. (1997). *Solid State Commun.* **101**, 835–839.
Hui, L., Yunchang, D., Jiongliang, Y. & Zeyun, W. (1995). *J. Power Sources*, **57**, 137–140.
Khan, A. I. & O'Hare, D. (2002). *J. Mater. Chem.* **12**, 3191–3198.
Louër, D. & Langford, J. I. (1988). *J. Appl. Cryst.* **21**, 430–437.
Liu, Z., Ma, R., Osada, M., Takada, K. & Sasaki, T. (2005). *J. Am. Chem. Soc.* **127**, 13869–13874.
Martin, M. J. S., Villa, M. V. & Camazano, M. S. (1999). *Clays Clay Miner.* **47**, 777–783.
Ogawa, M. & Kaiho, H. (2002). *Langmuir*, **18**, 4240–4242.
Olanrewaju, J., Newalker, B. L., Mancino, C. & Komarneni, S. (2000). *Mater. Lett.* **45**, 307–310.
Oswald, H. R. & Asper, R. (1977). *Preparation and Crystal Growth of Materials with Layered Structures*, edited by R. M. A. Lieth, Vol. 1, pp. 71–140. Amsterdam: D. Reidel.
Radha, A. V. & Kamath, P. V. (2003). *Bull. Mater. Sci.* **26**, 661–666.
Radha, A. V., Shivakumara, C. & Kamath, P. V. (2005). *Clays Clay Miner.* **53**, 521–528.
Ramesh, T. N., Jayashree, R. S. & Kamath, P. V. (2003). *Clays Clay Miner.* **51**, 570–576.
Reichle, W. T. (1986). *Solid State Ion.* **22**, 135–141.
Rodriguez-Carvajal, J. (2005). *FULLPROF*, .2k code, Version 3.3. http://www-llb.cea.fr/fullweb/powder.htm.
Seida, Y., Nakano, Y. & Nakamura, Y. (2002). *Clays Clay Miner.* **50**, 525–532.
Taylor, H. F. W. (1973). *Mineral. Mag.* **39**, 377–389.
Thomas, G. S. & Kamath, P. V. (2006). *J. Chem. Sci.* **118**, 127–133.
Thomas, G. S., Rajamathi, M. & Kamath, P. V. (2004). *Clays Clay Miner.* **52**, 693–699.
Tichit, D., Rolland, A., Prinetto, F., Fetter, G., de Jesus Martinez-Ortiz, M., Valenzuela, M. A. & Bosch, P. (2002). *J. Mater. Chem.* **12**, 3832–3838.
Treacy, M. M. J., Newsam, J. M. & Deem, M. W. (1991). *Proc. R. Soc. London Ser. A*, **433**, 499–520.
Treacy, M. M. J., Deem, M. W. & Newsam, J. M. (2000). *Computer code DIFFaX*, Version 1.807. http://www.public.asu.edu/~mtreacy/DIFFaX.html.
Verma, A. R. & Krishna, P. (1966). *Polymorphism and Polytypism in Crystals.* New York: John Wiley and Sons.
Zhao, Y., Li, F., Zhang, R., Evans, D. G. & Duan, X. (2002). *Chem. Mater.* **14**, 4286–4291.